Colloidally Stable Germanium Nanocrystals for Photonic Applications

Eric J. Henderson,[†] Makoto Seino,[‡] Daniel P. Puzzo,[†] and Geoffrey A. Ozin[†,*]

[†]Lash Miller Chemical Laboratories, Department of Chemistry, University of Toronto, 80 St. George Street, Toronto, Ontario, Canada M5S 3H6 and [‡]Solar Energy Division, Kaneka Corporation, 2-1-1, Hieitsuji, Otsu Shiga 520-0104, Japan

ARTICLE

ABSTRACT We report the development of a straightforward synthesis for colloidally stable germanium nanocrystals for use as a solution-processable precursor for the bottom-up fabrication of functional thin films. SiO_2-embedded germanium nanocrystals are produced by the reductive thermal processing of sol−gel glasses derived from mixtures of tetraethoxyorthogermanate (TEOG) and tetraethoxyorthosilicate (TEOS), and free-standing germanium nanocrystals are liberated from the encapsulating silicon dioxide through sequential chemical etching. The applicability of these germanium nanocrystals as a solution-processable thin film precursor is demonstrated by the fabrication of high refractive index thin films.

KEYWORDS: germanium · nanocrystals · sol−gel chemistry · thin films · refractive index · solution-processable · spin-coating

Semiconductor nanocrystals have captivated the imagination of scientists and engineers since their technological potential became evident over 2 decades ago. This is especially true for semiconductor quantum dots, in which quantum size effects and carrier confinement allow unprecedented control over optical and electronic properties.[1] Illuminating the way in this field, in both theoretical understanding and demonstrated applications, is indisputably the cadmium chalcogenide based II−VI quantum dots originally discovered by Brus.[2] However, legitimate concerns regarding their toxicity have yet to be resolved,[3] pressing for the advancement of alternate nontoxic technologies, including the group 14 semiconductor nanocrystals.[4]

Although silicon is the leader of the group 14 nanocrystal congeners, germanium (Ge) offers unique opportunities that are actively being pursued, especially for charge storage and infrared optical and optoelectronic applications.[5−7] Similarly to most semiconductor nanocrystals, focus has primarily been on Ge quantum dots, where size-dependent optical and electronic properties have been investigated mostly for optoelectronic or *in vivo* biological imaging applications.[8,9] However, what is perhaps an overlooked "nano advantage" is the solution-processability of colloidally stable nanomaterials for the production of structures which retain bulk properties, offering attractive alternatives to typical top-down fabrication techniques. Inexpensive, scalable, using nontoxic and easy to handle precursors, and requiring minimal infrastructure, spin-coating, dip-coating, and spray-coating, to name but a new, are certainly appealing thin film deposition methods, as long as the properties of the final material are suitable for the desired application. The applicability of this strategy has recently been demonstrated by the formation of highly conductive thin films and thin film transistors (TFTs) from solution-processable plasma-synthesized germanium nanocrystals (Ge-NCs).[10,11]

Since the first reports of luminescent Ge-NCs in 1991,[12] many syntheses have emerged based on surfactant/solvent-assisted solution reductions,[6,13−18] metathesis reactions,[19−21] supercritical thermolysis,[22,23] solution-phase thermal decomposition,[24−26] gas-phase plasma decomposition,[27] and solid-state thermolysis.[28,29] In almost all cases, emphasis has been placed on developing methods of controlling the average size of the Ge-NCs as well as obtaining narrow size distributions. This is not surprising given that the majority of foreseen applications for Ge-NCs, including optical, optoelectronic, and charge storage, are not only sensitive to the NC size but also to the size distribution.[30] As a result of these considerations, great care is taken during synthesis to ensure size uniformity, which oftentimes results in the use of elaborate experimental setups,

*Address correspondence to gozin@chem.utoronto.ca.

Received for review September 24, 2010 and accepted November 01, 2010.

Published online November 9, 2010.
10.1021/nn102521k

specialized reagents, surfactants, extensive cleaning, and lengthy precipitation steps.

As an example, consider the synthesis of SiO_2-embedded Ge-NCs, a system which continues to generate great interest for charge storage applications (*i.e.*, flash memory).[5,31,32] The vast majority of the reported syntheses are based on physical methods such as ion implantation,[33] chemical vapor deposition,[34] and co-sputtering.[35] However, a very elegant alternative synthetic method involves the co-hydrolysis and co-condensation of Si and Ge sol−gel precursors to form Si−Ge mixed oxide glasses. Considering that all of these methods require annealing in inert or H_2-containing atmospheres to reduce GeO_2 to Ge (in the case of H_2 atmospheres), initiate Ge diffusion through the encapsulating SiO_2 matrix, clustering of Ge atoms, and eventual crystallization of Ge-NCs, it is surprising that the sol−gel approach is not as frequently used. Such sol−gel systems can offer tremendous opportunities for NC size control, either by exploiting the compositional versatility of sol−gel chemistry or through simple changes to processing conditions (*i.e.*, peak temperature and time).[36−38] In order to obtain a narrow Ge-NC size distribution from the thermal processing of these sol−gel copolymers, their ideal structure would consist of a homogeneous distribution of Ge atoms throughout the copolymer. The first report of SiO_2-embedded Ge-NCs formed *via* sol−gel copolymers employed mixtures of $GeCl_4$ and $Si(OEt)_4$ (TEOS),[39] but the very fast hydrolysis rate of $GeCl_4$ relative to TEOS led to difficulties in making solid solutions, controlling the nucleation and growth reaction, and therefore the resulting size and size distribution of the Ge-NCs.[40] In order to overcome this kinetic obstacle, variations to the Ge sol−gel precursors have been used to slow the hydrolysis rate, using 3-trichlorogermanium propionic acid (Cl_3−Ge-C_2H_4−CO_2H) in particular.[36−38,40] Similar kinetic differences are likely the reason why combinations of the typical (and inexpensive) sol−gel precursors $Ge(OEt)_4$ (TEOG) and $Si(OEt)_4$ (TEOS) have not been used for SiO_2-embedded Ge-NCs. The greater hydrolysis rate of TEOG[41] would lead to GeO_2 clustering during co-hydrolysis and co-condensation and ultimately result in an inhomogeneous distribution (phase separation) of Ge throughout the sol−gel copolymer. This is especially surprising given the wealth of examples using TEOG/TEOS sol−gel for the formation of compositionally homogeneous index-controlled optical fibers.[41] Therefore, the necessity of controlled size and narrow size distribution in these advanced applications has the added cost of exotic precursors and elaborate reaction conditions, which removes the elegant simplicity of the sol−gel process.

There are, of course, applications that exploit the "nano-advantage" without being held hostage to size effects, and for these, the nanoparticle synthesis becomes much more straightforward. For example, it has recently been shown that dielectric nanoparticle suspensions can be used as solution-processable precursors for the bottom-up fabrication of porous distributed Bragg reflectors (Bragg mirrors).[42] Using commercially available nanoparticle suspensions with size distributions up to 20%, high quality Bragg mirrors have been fabricated with reflectance approaching 100%. As the nanoscaling laws and quantum size effects that govern optical and electronic phenomena in semiconductor quantum dots do not appreciably affect the dispersion relations of dielectrics in the visible spectrum to the same extent, narrow nanoparticle size distributions become less of a priority. In fact, broad size distributions could even lead to higher fill fractions and greater effective refractive indices. With a bulk refractive index $n > 4$, germanium has the potential to contribute greatly to the photonics field, especially with the development of colloidal, solution-based thin film fabrication techniques.

Here we present for the first time the synthesis of free-standing Ge-NCs obtained from the thermal processing of TEOG/TEOS sol−gel copolymers and their application as a solution-processable colloidally stable precursor for photonic applications. A sol−gel glass was synthesized *via* co-hydrolysis and co-condensation of TEOG and TEOS, and no special considerations were taken to control relative reaction rates. After aging and drying, thermal processing in a slightly reducing atmosphere resulted in the formation of a dark red/black powder from which Ge-NCs were liberated by sequential chemical etching steps. The resulting colloidally stable Ge-NCs were then used as a solution-processable precursor for the formation of high refractive index films.

RESULTS AND DISCUSSION

We present the synthesis of free-standing Ge-NCs *via* the thermal reduction of GeO_2/SiO_2 sol−gel copolymers obtained by co-hydrolysis and co-condensation of TEOG and TEOS and their use as a solution-processable colloidally stable precursor for high refractive index thin films. With this application in mind, this synthesis is a straightforward and cost-effective alternative to comparable sol−gel preparations in which great care is taken to ensure similar hydrolysis and condensation rates of the Ge and Si precursors, usually through compositional modifications to the sol−gel precursors.[38] We also demonstrate for the first time how sequential chemical etching steps can be used to liberate the Ge-NCs from the encapsulating matrix and produce colloidally stable free-standing Ge-NCs. We demonstrate the applicability of this system as a solution-processable precursor for the formation of high refractive index thin films.

The present synthetic strategy is based upon solid matrix-assisted nanocrystal formation and growth, a proven method for the preparation of various Group

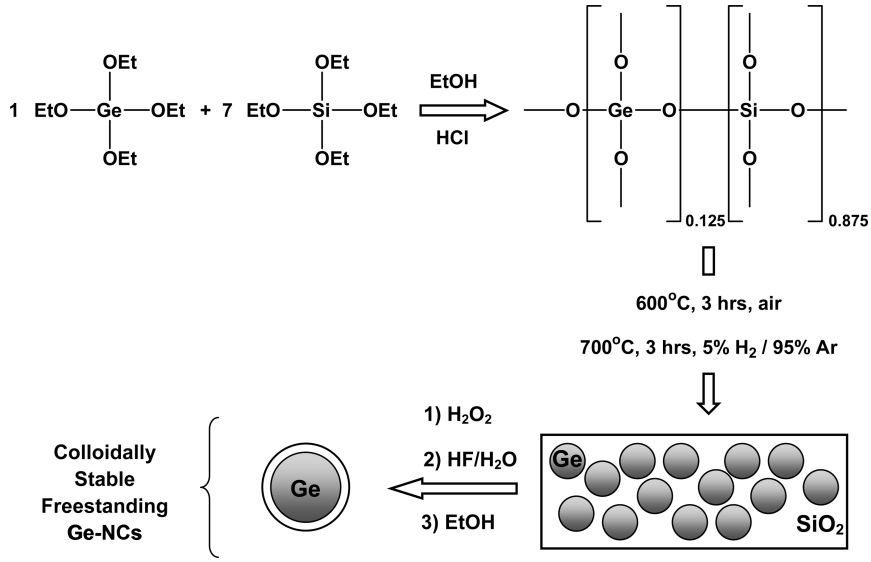

Scheme 1. Schematic outline of Ge-NC synthesis. Acid-catalyzed hydrolysis and co-condensation of TEOG and TEOS generates a compositionally tunable $[(SiO_2)_x(GeO_2)_y]_n$ sol−gel copolymer. In the present system, the TEOG/TEOS ratio was 1:7. After aging and drying at high temperatures in air, thermally induced reduction of GeO_2 by H_2 in the processing atmosphere generates elemental Ge that subsequently nucleates, grows, and crystallizes into Ge-NCs encapsulated in a SiO_2 matrix. Sequential etching steps to remove bulk unencapsulated Ge and the SiO_2 matrix generates free-standing Ge-NCs with mixed oxide/hydroxide/alkoxide surface termination that form stable suspensions in ethanol or methanol.

14 semiconductor nanocrystals, including Si, Ge, $Si_{1-x}Ge_x$, and SiC.[28,43−45] In these systems, a solid precursor with desired composition is prepared such that thermal initiation causes chemical transformations to the solid and activates thermodynamic driving forces that result in the diffusion of group 14 atoms throughout an inert encapsulating matrix. The matrix not only provides a temperature-resistant support for nanocluster crystallization, a key requirement for group 14 semiconductors that require high temperatures for crystallization, but also imposes kinetic diffusion barriers that can be exploited to accurately control nanocrystal formation and growth.

In the present synthesis, the formation of $[(GeO_2)_{0.125}(SiO_2)_{0.875}]_n$ copolymers is achieved *via* straightforward sol−gel processing of TEOG and TEOS (Scheme 1). The compositional versatility of sol−gel chemistry can be exploited to accurately control the composition of the resulting copolymer. In this way, copolymers with TEOG/TEOS ratios of 1:3, 1:5, and 1:7 were investigated, with the latter exhibiting optimal behavior. It is well-known that the hydrolysis and condensation rates of TEOG are greater than for TEOS,[41] which under the present experimental conditions leads to unavoidable formation of GeO_2 colloidal clusters and subsequent GeO_2-rich domains in the solid copolymer. It was found that, as the TEOG/TEOS ratio decreased, the formation of these GeO_2-rich domains was limited, as evidenced by the absence of crystalline GeO_2 reflections in XRD measurements (not shown).

The composition and structure of the $[(GeO_2)_{0.125}(SiO_2)_{0.875}]_n$ sol−gel copolymer was evaluated by Fourier transform infrared spectroscopy (FTIR) and Raman spectroscopy (Figure 1A−C). The FTIR spectrum (Figure 1A) is dominated by peaks centered at 1080 and 815 cm^{-1} attributed to vibrations of the oxide framework, broad −OH stretching centered at 3430 cm^{-1} from uncondensed Ge−OH and Si−OH groups, and low intensity C−H stretching at 2925 cm^{-1} from trace amounts of unhydrolyzed −OEt groups. Detailed examination of the oxide network vibrations (Figure 1B) allows their deconvolution into numerous vibrational modes,[46] including Si−O−Si stretching at *ca.* 1180 cm^{-1} (a) and *ca.* 1080 cm^{-1} (b), Si−O−Ge stretching at *ca.* 980 cm^{-1} (c), Ge−O−Ge stretching at *ca.* 980 cm^{-1} (c) and 800 cm^{-1} (d), Si−O−Si deformations at *ca.* 780 cm^{-1} (e), low intensity Si−O−Ge deformations at 670 cm^{-1} (f), and Ge−O−Ge deformations at *ca.* 520 cm^{-1} (g). These assignments are further supported by Raman spectroscopy (Figure 1C) in which the symmetric Si−O−Si stretching at *ca.* 470 cm^{-1} (h), Ge−OH stretching at 760 cm^{-1} (i), and Si−OH stretching at 962 cm^{-1} (j) are the prominent features. Low intensity shoulders at *ca.* 560 cm^{-1} corresponding to Ge−O−Si and Ge−O−Ge deformations and Ge−O−Si deformations at *ca.* 670 cm^{-1} are also present. Nearly identical spectral characteristics have been reported for SiO_2−GeO_2 gels prepared under similar conditions,[46] and the appearance of these diagnostic bands in the FTIR and Raman spectra confirm the presence of Si−O−Si, Si−O−Ge, and Ge−O−Ge units in the solid sol−gel copolymer.

Reductive thermal processing of the white solid $[(GeO_2)_{0.125}(SiO_2)_{0.875}]_n$ copolymer (Figure 2A) results in H_2 reduction of GeO_2 to Ge and the subsequent diffusion of Ge throughout the SiO_2 matrix, clustering, and eventual crystallization (Scheme 1). At this point, a dark red/black powder was obtained (Figure 2B), consisting

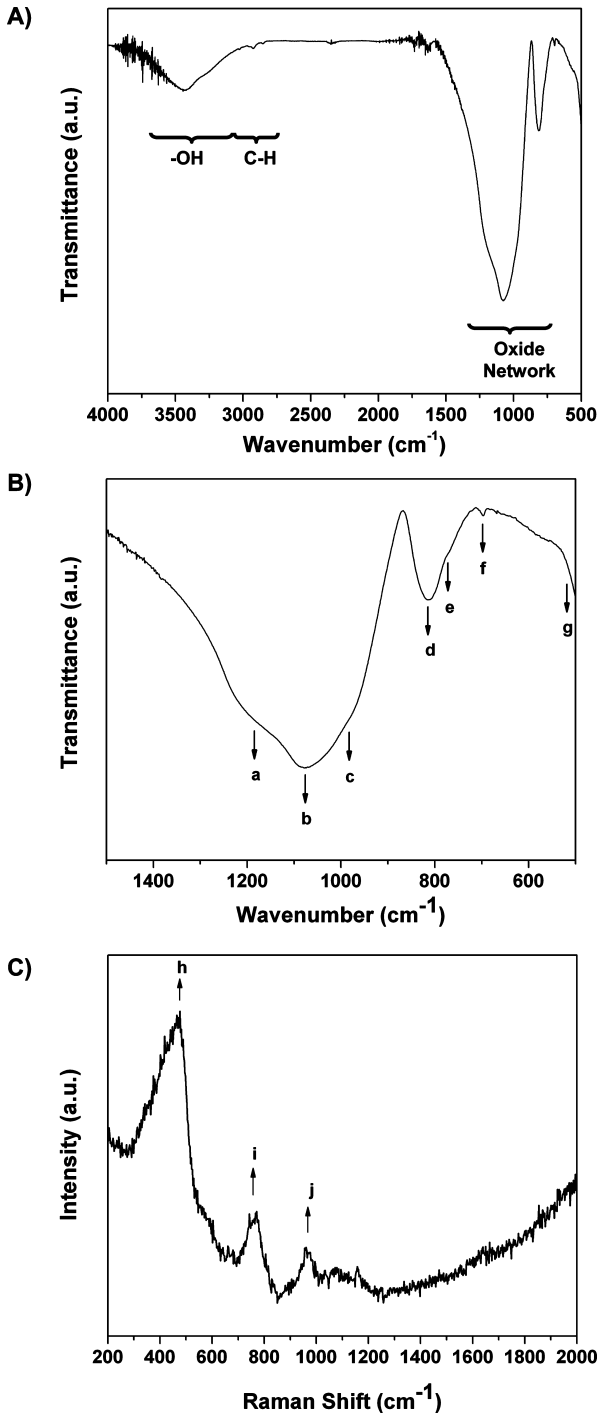

Figure 1. Characterization of $[(GeO_2)_{0.125}(SiO_2)_{0.875}]_n$ sol−gel copolymer. (A) Fourier transform infrared (FTIR) spectrum of $[(GeO_2)_{0.125}(SiO_2)_{0.875}]_n$ sol−gel copolymer dominated by vibrations of the oxide network, −OH stretching from uncondensed Ge−OH and Si−OH groups, and low intensity C−H stretching from unhydrolyzed −OEt group. (B) Detailed examination of the network vibrations showing characteristic Si−O−Si stretching (a and b), Si−O−Ge stretching (c), Ge−O−Ge stretching (c and d), Si−O−Si deformations (e), low intensity Si−O−Ge deformations (f), and Ge−O−Ge deformations (g). (C) Raman spectrum of $[(GeO_2)_{0.125}(SiO_2)_{0.875}]_n$ sol−gel copolymer showing Si−O−Si stretching (h), Ge−OH stretching (i) and Si−OH stretching (j).

of two classes of crystalline Ge and the SiO_2 matrix. Bulk crystalline Ge forms from the reduction of the aforementioned GeO_2-rich domains in the sol−gel copolymer and gives rise to the black color of the powder. Bulk crystals, as opposed to nanocrystals, result because their formation and growth in not directed by an encapsulating SiO_2 matrix. Ge-NCs are produced from the reduction of Ge oxide species dispersed throughout the SiO_2 matrix and form *via* a diffusion-mediated mechanism. These Ge-NCs are encapsulated within the SiO_2 and give rise to the red color of the powder owing to quantum size effects on the NC band gap and absorption properties.

Although the formation of two classes of crystalline Ge could be seen as problematic, the fact that only the Ge-NCs are encapsulated within a protective SiO_2 matrix can be exploited to selectively remove the bulk Ge impurities. Chemical etching of bulk Ge by aqueous H_2O_2 has previously been shown to be an effective strategy for its selective dissolution from SiO_2 composites.[44] As a result of this H_2O_2 etching step, the black powder turns into a deep red powder (Figure 2C), consisting exclusively of SiO_2-encapsulated Ge-NCs.

The thermal transformation of the $[(GeO_2)_{0.125}(SiO_2)_{0.875}]_n$ sol−gel copolymer into SiO_2-embedded Ge-NCs and subsequent removal of bulk Ge impurities was monitored by powder X-ray diffraction (PXRD) (Figure 2D). The white sol−gel precursor shows a single broad reflection in the PXRD pattern centered at *ca.* 22°, arising from the predominantly amorphous SiO_2 network.[47] The formation of crystalline Ge after thermal processing at 700 °C in 5% H_2/95% Ar to reduce the GeO_2 to Ge is confirmed by the appearance of intense sharp reflections in the XRD pattern centered at *ca.* 27, 45, 53, and 66° characteristic of the (111), (220), (311), and (400) crystal planes of diamond structure Ge.[48] Although the dark red/black powder contains both bulk and nanocrystalline Ge, the former dominates the XRD pattern, as diffraction peak widths are naturally biased to large crystal sizes.[49] After selective removal of the bulk Ge from the composite material by H_2O_2 etching, a clear change in the XRD pattern is seen for the deep red powder. Broad low intensity crystalline Ge reflections appear above the amorphous background, characteristic of SiO_2-embedded Ge-NCs.

In order to liberate the Ge-NCs from the encapsulating SiO_2 matrix, aqueous hydrofluoric acid (HF) solutions were used. This approach has previously been employed to liberate Ge nanostructures from SiO_2.[50] The etching chemistry of SiO_2 by HF is well-understood and provides an effective means by which to remove the matrix. However, the effect of HF on crystalline Ge surfaces is complex and not as well-understood, with short-lived Ge−H species succumbing to oxidation and hydrolysis.[51] In our experience, the use of alcohol additives during etching, especially ethanol, provided excellent colloidal stability to the liberated Ge-NCs, likely through ethoxide surface passivation. Detailed investigations into the surface chemistry of these NCs is

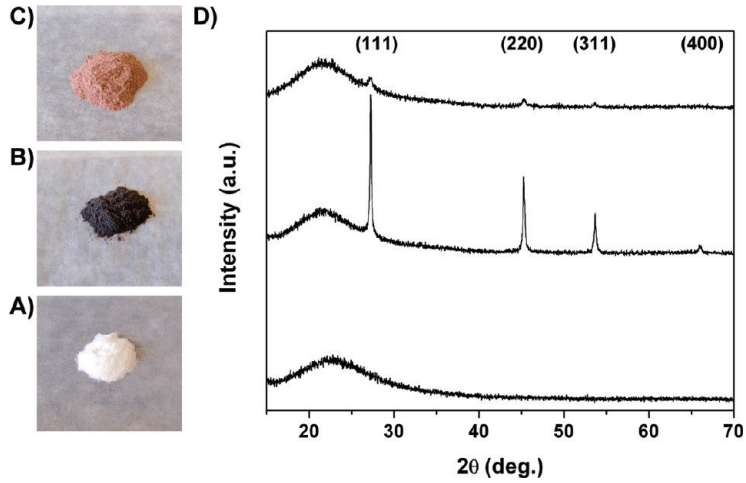

Figure 2. Transformation of $[(GeO_2)_{0.125}(SiO_2)_{0.875}]_n$ sol−gel copolymer into SiO_2-embedded Ge-NCs. Picture of $[(GeO_2)_{0.125}(SiO_2)_{0.875}]_n$ sol−gel copolymer (A) after processing at 600 °C and consisting of a SiO_2/GeO_2 mixed oxide network, (B) after processing at 700 °C in 5% H_2/95% Ar and consisting of a mixture of bulk crystalline Ge and SiO_2-encapsulated Ge-NCs, and (C) after H_2O_2 etching to remove bulk crystalline Ge and consisting exclusively of SiO_2-embedded Ge-NCs. (D) Evolution of XRD pattern showing reflections characteristic of diamond structure Ge. The traces correspond to the associated samples shown in pictures A−C.

currently underway in our laboratories. The free-standing Ge-NCs form deep red colloidal suspensions in ethanol and methanol with only limited flocculation and precipitation occurring over periods of several weeks (Figure 3A,B). The absorption spectrum (Figure 3C) shows an onset in the infrared at *ca.* 1200 nm, a prominent shoulder at *ca.* 500 nm, and a rising absorption edge into the UV, giving the present Ge-NCs their characteristic red color. The gradual onset and increase in the infrared absorption likely results from the appreciable size distribution in the present Ge-NCs as determined from TEM measurements. Photoluminescence (PL) emission was not observed in the present Ge-NCs, as the measured mean diameter is greater than the Bohr exciton radius in bulk Ge and, as such, quantum confinement effects are unappreciable.

The Raman spectrum of free-standing Ge-NCs (Figure 4A) drop-cast from ethanol onto a glass microscope slide shows a single asymmetric peak centered at 298.5 cm^{-1} corresponding to the optical phonon (OP) in crystalline Ge. In the bulk crystal, the phonon vibration occurs at a frequency of *ca.* 302 cm^{-1}, and the shift to lower frequencies in the present sample and the asymmetric broadening are attributed to the phonon confinement effect in the Ge-NCs.[52] The PXRD pattern of the free-standing Ge-NCs drop-cast from ethanol onto a low intensity background Si wafer (Figure 4B) shows intense broad reflections characteristic of diamond structure Ge. Scherrer analysis of the XRD peak broadening provided approximate mean crystal diameters of 14 nm. It should be noted that the absence of the broad feature attributed to amorphous SiO_2 is consistent with the liberation of the Ge-NCs and etching of the encapsulating matrix. Transmission electron microscopy (TEM) images of Ge-NCs drop-cast onto a holey carbon grid (Figure 4C) show spherical NCs with a measured mean diameter of 17.7 nm ($n = 448$; $\sigma = 5.5$ nm, 31%), in agreement with Scherrer analysis of XRD peak

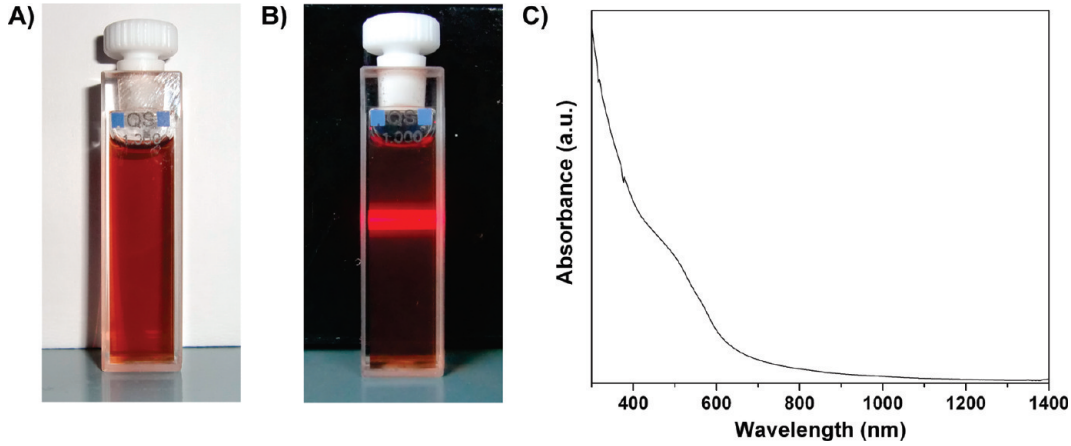

Figure 3. (A) Picture of free-standing, colloidally stable Ge-NCs in ethanol. (B) Scattering of a red laser from colloidally stable Ge-NCs in ethanol. (C) Absorption spectrum of Ge-NCs dispersed in ethanol showing an onset at *ca.* 1200 nm, a prominent shoulder at *ca.* 500 nm, and a rising absorption edge into the UV.

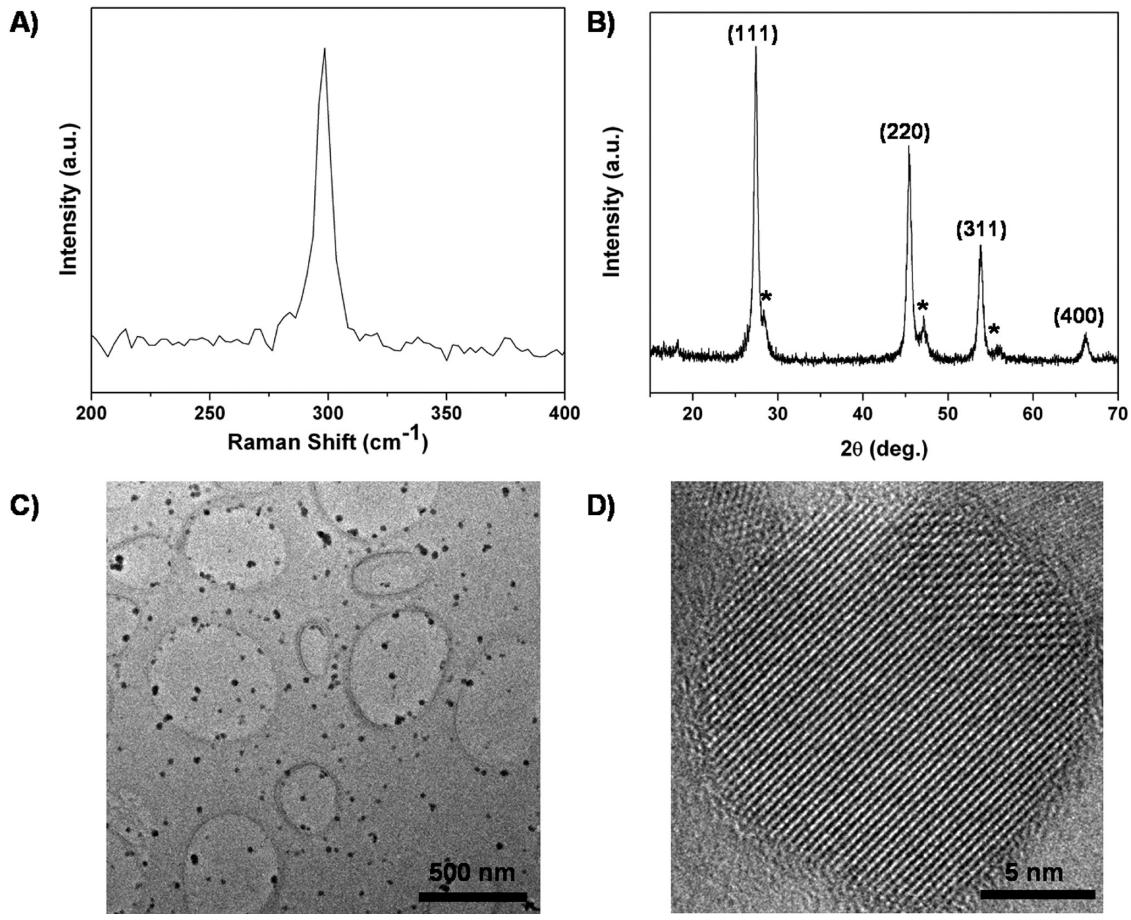

Figure 4. Characterization of free-standing colloidally stable Ge-NCs. (A) Microscope Raman spectrum of free-standing Ge-NCs drop-cast from ethanol onto a glass microscope slide showing the crystalline Ge optical phonon (OP). (B) Powder X-ray diffraction (PXRD) pattern of Ge-NCs drop-cast onto a low intensity background Si wafer showing reflections characteristic of diamond structure Ge (* denotes reflections from substrate). (C) Representative transmission electron microscope (TEM) images of Ge-NCs drop-cast from ethanol onto a holey carbon grid. The measured mean diameter was 17.7 nm (n = 448; σ = 5.5 nm, 31%). (D) High-resolution TEM image showing lattice fringes corresponding to the (111) crystal planes of diamond structure Ge.

broadening. As previously mentioned, the substantial size distribution in the present system is likely the result of compositional inhomogeneities in the sol−gel precursor arising from kinetic differences in TEOS and TEOG hydrolysis and condensation. High-resolution TEM (HRTEM) (Figure 4D) of a single isolated Ge-NC clearly shows crystalline lattice fringes that extend throughout the entire structure and an amorphous surface layer that likely arises from oxide, hydroxide, and alkoxide species. The measured lattice spacing was 0.32 nm corresponding to the (111) crystal plane interlayer spacing in diamond structure Ge.[48] Finally, the composition of the Ge-NCs was verified by energy-dispersive X-ray spectroscopy (EDX) (Supporting Information, SI1), which confirms that the NCs are composed predominantly of Ge, with trace O arising from the aforementioned surface species.

The applicability of the present colloidal Ge-NCs as a solution-processable precursor for bottom-up fabrication was demonstrated by the formation of thin films by spin-coating. In order to prepare thin films, a 0.5 wt % solution of Ge-NCs in methanol was spun-cast onto Si wafers, and the film was characterized by cross-sectional scanning electron microscopy (SEM) and spectroscopic elipsometry. Methanol was used as the solvent as opposed to ethanol, as the greater volatility produced thicker, higher quality films. In this manner, high quality films of 150 nm thickness were obtained. From the cross-sectional SEM imaging (Figure 5A), it is clear that the film is of even thickness with a uniform surface. The slight texturing of the surface and noticeable porosity arise from the interparticle void spaces, a well-known phenomenon in nanoparticle-based thin films.[42]

In order to determine the thickness as well as the energy dispersion of the real and imaginary parts of the refractive index of the Ge-NC thin films, spectroscopic ellipsometry measurements were performed at an angle of 75° over a wavelength range of 1.27−4.0 eV. A Tauc−Lorentz model, which is based on the Tauc joint density of states and the Lorentz model for the dielectric response for a collection of single atoms, was used for the parametrization of the dielectric function of the Ge-NC thin films.[53] According to the model, if only a single transition is considered, then the imaginary part

of the dielectric function is given by

$$\varepsilon_2(E)\begin{cases} = \dfrac{AE_0C(E-E_g)^2}{(E^2-E_0^2)^2+C^2E^2}\cdot\dfrac{1}{E} & \text{when } E > E_g \\ = 0 & \text{when } E > E_g \end{cases} \quad (1)$$

where A is the amplitude, C the broadening, and E_o the central position of the transition. E_g is the energy gap, and $\varepsilon_1(\infty)$ is a constant that corresponds to the contribution of transitions outside the measured spectral range. The extinction coefficient k is readily obtained from ε_2, while the real part of the dielectric constant is obtained by Kramers−Kronig integration:

$$\varepsilon_1(E) = \varepsilon_1(\infty) + \frac{2}{\pi}P\int_{E_g}^{\infty}\frac{\xi\varepsilon_2(\xi)}{\xi^2-E^2}d\xi \quad (2)$$

In this case, P denotes the Cauchy principal value and ξ is a function related to the complex angular frequency. The fitting was performed using Levenberg−Marquardt logarithm where six parameters were fitted: the thickness and the four TL parameters. The R^2 value of the regression analysis for the multilayer structure was >0.98, and the resulting energy dispersion is shown in Figure 5B. It should be mentioned that no Bruggemann effective medium approximation was necessary (typically employed to account for roughened interfaces) in order to improve the statistical measure of the fitting, attesting to the high quality and smoothness of the present films. The most noteworthy features of this energy dispersion are the large n at infrared wavelengths and the appreciable absorption, k, throughout the visible as well as UV wavelength ranges. The former is encouraging for the fabrication of bottom-up photonic crystals operating at infrared wavelengths and the latter for the preparation of solution-processable electrical and optoelectronic devices, both ongoing projects in our laboratory.

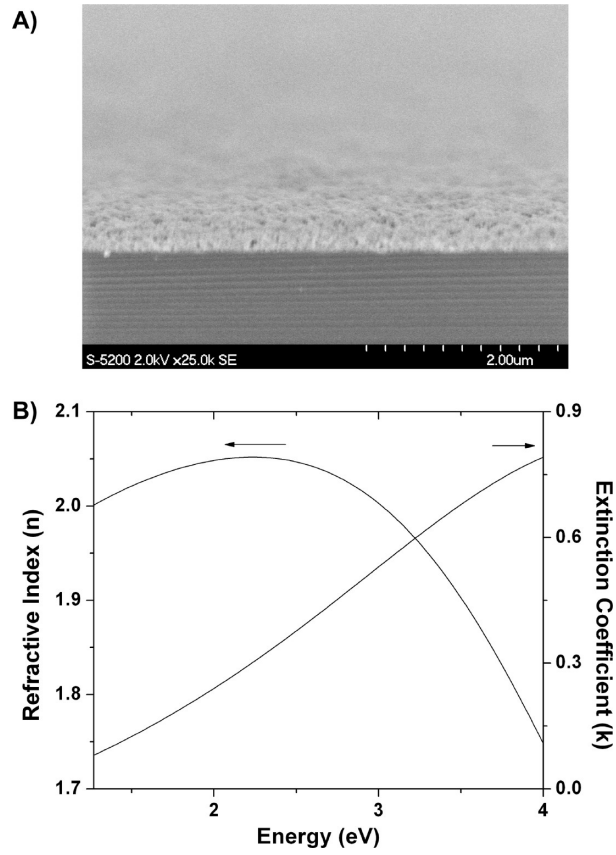

Figure 5. Ge-NC thin film. (A) Representative cross-sectional SEM image of a spun-cast Ge-NC thin film showing a uniform layer thickness and slightly textured surface with noticeable porosity arising from the interparticle void spaces. (B) Refractive index (n) and extinction coefficient (k) obtained from a Tauc−Lorentz model of the spectroscopic ellipsometric measurements of a spun-cast Ge-NC thin film. The Tauc−Lorentz parameters obtained include the film thickness = 151 nm, A = 16.02, $\varepsilon_1(\infty)$ = 1.562 eV, E_o = 4.387 eV, C = 4.439 eV, and E_g = 0.63 eV.

CONCLUSION

We have developed a straightforward synthesis for colloidally stable Ge-NCs for use as a solution-processable precursor for the bottom-up fabrication of functional thin films. For the first time, SiO_2-embedded Ge-NCs are produced by the reductive thermal processing of sol−gel glasses derived from mixtures of tetraethoxyorthogermanate (TEOG) and tetraethoxyorthosilicate (TEOS). A two-step chemical etching protocol was also developed in order to liberate free-standing Ge-NCs from the encapsulating oxide, which demonstrated excellent colloidal stability in alcohol solvents. The applicability of these Ge-NCs as a solution-processable thin film precursor is demonstrated by the fabrication of high refractive index thin films.

EXPERIMENTAL METHOD

Reagents and Materials. Tetraethoxyorthogermanate (TEOG, 99.95%) and tetraethoxyorthosilicate (TEOS, 98%) were purchased from Aldrich and used as received. Anhydrous ethanol was purchased from Brampton and used as received. Hydrochloric acid ($HCl_{(aq)}$, 37%) was obtained from Riedel-de Haën. Hydrogen peroxide ($H_2O_{2(aq)}$, 35%) and hydrofluoric acid ($HF_{(aq)}$, 48%) were purchased from Caledon and used as received.

Synthesis of $[(GeO_2)_{0.125}(SiO_2)_{0.875}]_n$ Sol−Gel Copolymer. TEOG (3.64 g, 14.4 mmol), TEOS (21.0 g, 100.8 mmol) (1:7 ratio), and anhydrous ethanol (40 mL) were added to a round-bottom flask equipped with a magnetic stir bar, and the solution was gently stirred in air for 30 min to ensure a high degree of mixing. After this time, aqueous HCl (0.01 M, 20 mL) was added to the solution to catalyze hydrolysis and condensation reactions. The clear and colorless solution turned cloudy white after addition of the HCl solution, and generated a white gel after 48 h. The gel was heated in air at 100 °C in a conventional oven for 48 h and subsequently heated at 600 °C in air for 3 h to complete condensation and dry the solid copolymer. The resulting solid $[(GeO_2)_{0.125}(SiO_2)_{0.875}]_n$ sol−gel copolymer (7.56 g) was mechanically ground in a mortar and pestle to give a fine white powder.

Ge-NC/SiO_2 Composite Preparation. Solid $[(GeO_2)_{0.125}(SiO_2)_{0.875}]_n$ sol−gel copolymer (2.0 g) was placed in a quartz reaction boat and transferred to a high-temperature tube furnace. The copolymer was heated from 25 to 700 °C at 17 °C/min in a slightly re-

ducing atmosphere (5% H_2/95% Ar) at which point the temperature was held for 3 h. After cooling to room temperature, the dark red/black powder (1.80 g) was stirred vigorously in a mixture of water (60 mL) and hydrogen peroxide (120 mL) for 30 min to etch bulk unencapsulated Ge. The resulting deep red powder was isolated by centrifugation and washed twice each with water and ethanol and finally dried under flowing N_2 to give bulk Ge-NC/SiO_2 composite (1.53 g).

Liberation of Ge-NCs. Free-standing Ge-NCs were liberated from the encapsulating matrix by etching the SiO_2 in a mixture of ethanol and aqueous HF. In a typical experiment, Ge-NC/SiO_2 composite (1.0 g) was stirred in a mixture of water (10 mL), ethanol (10 mL), and 48% $HF_{(aq)}$ (10 mL) for 15 min. As the reaction proceeded, the formation of $SiF_{4(g)}$ from the etching of SiO_2 by HF was evident. A dark red solid was isolated by centrifugation and washed twice each with water and ethanol to give free-standing Ge-NCs (3 mg), which formed stable deep red colloidally stable suspensions in ethanol. The final solvent can easily be changed during the last washing steps (*e.g.*, substitute ethanol for methanol).

Preparation of Ge-NC Films. In order to prepare thin films, a 0.5 wt % solution of Ge-NCs in methanol was first sonicated for several hours. At the dispensing stage in the spin-coating process, the Ge-NC dispersion was filtered through a 0.7 μm pore Titan 2 GL Microfiber syringe filter to remove any aggregated material. Dispersions were spin-coated at a speed of 1000 rpm for 120 s.

Characterization. FTIR spectroscopy was performed on a Perkin-Elmer Spectrum One FTIR spectrometer. Solid $[(GeO_2)_{0.125}(SiO_2)_{0.875}]_n$ sol−gel copolymer was mixed with KBr, ball milled into a fine power, and pressed into a dense pellet for analysis. Raman spectroscopy was performed using a 532 nm diode laser and calibrated using a crystalline silicon wafer. X-ray diffraction patterns of all samples were obtained on low intensity background substrates and acquired using a Siemens D5000. Low-resolution and HRTEM imaging and EDX spectroscopy were performed at the Canadian Centre for Electron Microscopy at McMaster University using a FEI Titan 80−300 keV electron microscope. TEM samples of Ge-NCs were drop-cast from an ethanol suspension onto a holey carbon coated copper grid. Absorption spectroscopy of ethanol suspensions of Ge-NCs was performed on a Perkin-Elmer UV/vis/NIR spectrometer Lambda 900. The spin-coater used to deposit films of Ge-NCs was a Laurell WS-400A-6NPP/LITE. Spectroscopic ellipsometry analyses were performed on a Sopra GES-5E ellipsometric porosimeter at a fixed incidence angle of 75° in the range of 1.27−4.0 eV. The modeling and regression of the ellipsometric spectra were performed using the software Winelli II provided by the ellipsometer manufacturer.

Acknowledgment. G.A.O. is the Government of Canada Research Chair in Materials Chemistry and Nanochemistry. We thank the Natural Sciences and Engineering Research Council (NSERC) of Canada for financial support of this work. We also thank S. Fukuda and T. Suezaki and Kaneka cooperation of Japan for financial support and useful discussions. L. Sandilands is thanked for assistance with Raman spectroscopy, S. Petrov for XRD measurements, C. Andrei and the Canadian Centre for Electron Microscopy for HRTEM imaging.

Supporting Information Available: Composition of free-standing Ge-NCs. This material is available free of charge *via* the Internet at http://pubs.acs.org.

REFERENCES AND NOTES

1. Alivisatos, A. P. Semiconductor Clusters, Nanocrystals, and Quantum Dots. *Science* **1996**, *271*, 933–937.
2. Rossetti, R.; Nakahara, S.; Brus, L. E. Quantum Size Effects in the Redox Potentials, Resonance Raman Spectra, and Electronic Spectra of CdS Crystallites in Aqueous Solution. *J. Chem. Phys.* **1983**, *79*, 1086–1088.
3. Derfus, A. M.; Chan, W. C. W.; Bhatia, S. N. Probing the Cytotoxicity of Semiconductor Quantum Dots. *Nano Lett.* **2004**, *4*, 11–18.
4. Alsharif, N. H.; Berger, C. E. M.; Varanasi, S. S.; Chao, Y.; Horrocks, B. R.; Datta, H. K. Alkyl-Capped Silicon Nanocrystals Lack Cytotoxicity and Have Enhanced Intracellular Accumulation in Malignant Cells *via* Cholesterol-Dependent Endocytosis. *Small* **2009**, *5*, 221–228.
5. Choi, W. K.; Chim, W. K.; Heng, C. L.; Teo, L. W.; Ho, V.; Ng, V.; Antoniadis, D. A.; Fitzgerald, E. A. Observation of Memory Effect in Germanium Nanocrystals Embedded in an Amorphous Silicon Oxide Matrix of a Metal-Insulator-Semiconductor Structure. *Appl. Phys. Lett.* **2002**, *80*, 2014.
6. Lee, D. C.; Pietryga, J. M.; Robel, I.; Werder, D. J.; Schaller, R. D.; Klimov, V. I. Colloidal Synthesis of Infrared-Emitting Germanium Nanocrystals. *J. Am. Chem. Soc.* **2009**, *131*, 3436–3437.
7. Ma, X.; Yuan, B.; Yan, Z. The Photodetector of Ge Nanocrystals/Si for 1.55 um Operation Deposited by Pulsed Laser Deposition. *Opt. Commun.* **2006**, *260*, 337–339.
8. Prabakar, S.; Shiohara, A.; Hanada, S.; Fujioka, K.; Yamamoto, K.; Tilley, R. D. Size Controlled Synthesis of Germanium Nanocrystals by Hydride Reducing Agents and Their Biological Applications. *Chem. Mater.* **2010**, *22*, 482–486.
9. Lambert, T. N.; Andrews, N. L.; Gerung, H.; Boyle, T. J.; Oliver, J. M.; Wilson, B. S.; Han, S. M. Water-Soluble Germanium(0) Nanocrystals: Cell Recognition and Near-Infrared Photothermal Conversion Properties. *Small* **2007**, *3*, 691–699.
10. And, Z. C. H.; Kortshagen, U. R. Solution-Processed Germanium Nanocrystal Thin Films as Materials for Low-Cost Optical and Electronic Devices. *Langmuir* **2009**, *25*, 11883–11889.
11. Holman, Z. C.; Liu, C. Y.; Kortshagen, U. R. Germanium and Silicon Nanocrystal Thin-Film Field-Effect Transistors from Solution. *Nano Lett.* **2010**, *10*, 2661–2666.
12. Maeda, Y.; Tsukamoto, N.; Yazawa, Y.; Kanemitsu, Y.; Masumoto, Y. Visible Photoluminescence of Ge Microcrystals Embedded in SiO_2 Glassy Matrices. *Appl. Phys. Lett.* **1991**, *59*, 3168–3170.
13. Lu, X.; Korgel, B. A.; Johnston, K. P. High Yield of Germanium Nanocrystals Synthesized from Germanium Diiodide in Solution. *Chem. Mater.* **2005**, *17*, 6479–6485.
14. Heath, J. R.; Shiang, J. J.; Alivisatos, A. P. Germanium Quantum Dots: Optical Properties and Synthesis. *J. Chem. Phys.* **1994**, *101*, 1607–1615.
15. Wilcoxon, J. P.; Provencio, P. P.; Samara, G. A. Synthesis and Optical Properties of Colloidal Germanium Nanocrystals. *Phys. Rev. B* **2001**, *64*, 0354171–0354179.
16. Warner, J. H.; Tilley, R. D. Synthesis of Water-Soluble Photoluminescent Germanium Nanocrystals. *Nanotechnology* **2006**, *17*, 3745–3749.
17. Warner, J. H. Solution-Phase Synthesis of Germanium Nanoclusters Using Sulfur. *Nanotechnology* **2006**, *17*, 5613–5619.
18. Fok, E.; Shih, M.; Meldrum, A.; Veinot, J. G. C. Preparation of Alkyl-Surface Functionalized Germanium Quantum Dots *via* Thermally Initiated Hydrogermylation. *Chem. Commun.* **2004**, *10*, 386–387.
19. Taylor, B. R.; Kauzlarich, S. M.; Lee, H. W. H.; Delgado, G. R. Solution Synthesis of Germanium Nanocrystals Demonstrating Quantum Confinement. *Chem. Mater.* **1998**, *10*, 22–24.
20. Taylor, B. R.; Kauzlarich, S. M.; Delgado, G. R.; Lee, H. W. H. Solution Synthesis and Characterization of Quantum Confined Ge Nanoparticles. *Chem. Mater.* **1999**, *11*, 2493–2500.
21. Taylor, B. R.; Fox, G. A.; Hope-Weeks, L. J.; Maxwell, R. S.; Kauzlarich, S. M.; Lee, H. W. H. Solution Preparation of Ge Nanoparticles with Chemically Tailored Surfaces. *Mater. Sci. Eng., B* **2002**, *96*, 90–93.
22. Lu, X.; Ziegler, K. J.; Ghezelbash, A.; Johnston, K. P.; Korgel, B. A. Synthesis of Germanium Nanocrystals in High Temperature Supercritical Fluid Solvents. *Nano Lett.* **2004**, *4*, 969–974.

23. Lu, X.; Korgel, B. A.; Johnston, K. P. Synthesis of Germanium Nanocrystals in High Temperature Supercritical CO_2. *Nanotechnology* **2005**, 16.
24. Wu, H. P.; Ge, M. Y.; Yao, C. W.; Wang, Y. W.; Zeng, Y. W.; Wang, L. N.; Zhang, G. Q.; Jiang, J. Z. Blue Emission of Ge Nanocrystals Prepared by Thermal Decomposition. *Nanotechnology* **2006**, *17*, 5339–5343.
25. Zaitseva, N.; Dai, Z. R.; Grant, C. D.; Harper, J.; Saw, C. Germanium Nanocrystals Synthesized in High-Boiling-Point Organic Solvents. *Chem. Mater.* **2007**, *19*, 5174–5178.
26. Gerung, H.; Bunge, S. D.; Boyle, T. J.; Brinker, C. J.; Han, S. M. Anhydrous Solution Synthesis of Germanium Nanocrystals from the Germanium(II) Precursor $Ge[N(SiMe_3)_2]_2$. *Chem. Commun.* **2005**, 1914–1916.
27. Gresback, R.; Holman, Z.; Kortshagen, U. Nonthermal Plasma Synthesis of Size-Controlled, Monodisperse, Freestanding Germanium Nanocrystals. *Appl. Phys. Lett.* **2007**, 91.
28. Henderson, E. J.; Hessel, C. M.; Veinot, J. G. C. Synthesis and Photoluminescent Properties of Size-Controlled Germanium Nanocrystals from Phenyl Trichlorogermane-Derived Polymers. *J. Am. Chem. Soc.* **2008**, *130*, 3624–3632.
29. Henderson, E. J.; Hessel, C. M.; Cavell, R. G.; Veinot, J. G. C. How Processing Atmosphere Influences the Evolution of GeO_2-Embedded Germanium Nanocrystals Obtained from the Thermolysis of Phenyl Trichlorogermane-Derived Polymers. *Chem. Mater.* **2010**, *22*, 2653–2661.
30. Heitmann, J.; Müller, F.; Zacharias, M.; Gösele, U. Silicon Nanocrystals: Size Matters. *Adv. Mater.* **2005**, *17*, 795–803.
31. Ang, R.; Chen, T. P.; Yang, M.; Wong, J. I.; Yi, M. D. The Charge Trapping and Memory Effect in SiO_2 Thin Films Containing Ge Nanocrystals. *J. Phys. D* **2010**, *43*, 015102.
32. Yang, M.; Chen, T. P.; Liu, Z.; Wong, J. I.; Zhang, W. L.; Zhang, S.; Liu, Y. Effect of Annealing on Charge Transfer in Ge Nanocrystal Based Nonvolatile Memory Structure. *J. Appl. Phys.* **2009**, *106*, 103701.
33. Zhang, J. Y.; Bao, X. M.; Ye, Y. H. Synthesis of Ge Nanocrystals in Thermal SiO_2 Films by Ge+ Ion Implantation. *Thin Solid Films* **1998**, *323*, 68–71.
34. Dutta, A. K. Visible Photoluminescence from Ge Nanocrystal Embedded into a SiO_2 Matrix Fabricated by Atmospheric Pressure Chemical Vapor Deposition. *Appl. Phys. Lett.* **1996**, *68*, 1189–1191.
35. Maeda, Y. Visible Photoluminescence from Nanocrystallite Ge Embedded in a Glassy SiO_2 Matrix: Evidence in Support of the Quantum-Confinement Mechanism. *Phys. Rev. B* **1995**, *51*, 1658–1670.
36. Yang, H.; Yang, R.; Wan, X.; Wan, W. Structure and Photoluminescence of Ge Nanoparticles with Different Sizes Embedded in SiO_2 Glasses Fabricated by a Sol-Gel Method. *J. Cryst. Growth* **2004**, *261*, 549–556.
37. Yang, H.; Yao, X.; Xie, S.; Wang, X.; Liu, S.; Fang, Y.; Gu, X.; Wang, F. Structure and Photoluminescence of Ge Nanoparticles Embedded in SiO_2 Gel Glasses Fabricated at Different Temperatures. *Opt. Mater.* **2005**, *27*, 725–730.
38. Yang, H.; Yao, X.; Wang, X.; Xie, S.; Fang, Y.; Liu, S.; Gu, X. Sol−Gel Preparation and Photoluminescence of Size Controlled Germanium Nanoparticles Embedded in a SiO_2 Matrix. *J. Phys. Chem. B* **2003**, *107*, 13319–13322.
39. Nogami, M.; Abe, Y. Sol−Gel Method for Synthesizing Visible Photoluminescent Nanosized Ge-Crystal-Doped Silica Glasses. *Appl. Phys. Lett.* **1994**, *65*, 2545–2547.
40. Yang, H.; Wang, X.; Shi, H.; Xie, S.; Wang, F.; Gu, X.; Yao, X. Photoluminescence of Ge Nanoparticles Embedded in SiO_2 Glasses Fabricated by a Sol−Gel Method. *Appl. Phys. Lett.* **2002**, *81*, 5144–5146.
41. *Handbook of Sol-Gel Science and Technology: Processing, Characterization and Applications*; Springer Reference: Berlin, 2005; Vol. 1.
42. Puzzo, D. P.; Bonifacio, L. D.; Oreopoulos, J.; Yip, C. M.; Manners, I.; Ozin, G. A. Color from Colorless Nanomaterials: Bragg Reflectors Made of Nanoparticles. *J. Mater. Chem.* **2009**, *19*, 3500–3506.
43. Henderson, E. J.; Kelly, J. A.; Veinot, J. G. C. Influence of $HSiO_{1.5}$ Sol−Gel Polymer Structure and Composition on the Size and Luminescent Properties of Silicon Nanocrystals. *Chem. Mater.* **2009**, *21*, 5426–5434.
44. Henderson, E. J.; Veinot, J. G. C. Synthesis of Oxide Encapsulated and Freestanding Hydride Surface Terminated $Si_{1-x}Ge_x$ Nanocrystals. *Chem. Mater.* **2007**, *19*, 1886–1888.
45. Henderson, E. J.; Veinot, J. G. C. From Phenylsiloxane Polymer Composition to Size-Controlled Silicon Carbide Nanocrystals. *J. Am. Chem. Soc.* **2009**, *131*, 809–815.
46. Mukherjee, S. P.; Sharma, S. K. Structural Studies of Gels and Gel-Glasses in the SiO_2- GeO_2 System Using Vibrational Spectroscopy. *J. Am. Ceram. Soc.* **1986**, *69*, 806–810.
47. Hessel, C. M.; Henderson, E. J.; Veinot, J. G. C. Hydrogen Silsesquioxane: A Molecular Precursor for Nanocrystalline Si-SiO_2 Composites and Freestanding Hydride-Surface-Terminated Silicon Nanoparticles. *Chem. Mater.* **2006**, *18*, 6139–6146.
48. Carpenter, J. P.; Lukehart, C. M.; Henderson, D. O.; Mu, R.; Jones, B. D.; Glosser, R.; Stock, S. R.; Wittig, J. E.; Zhu, J. G. Formation of Crystalline Germanium Nanoclusters in a Silica Xerogel Matrix from an Organogermanium Precursor. *Chem. Mater.* **1996**, *8*, 1268–1274.
49. Cullity, B. D.; Stock, S. R. *Elements of X-Ray Diffraction*, 3rd ed.; Prentice Hall: New York, 2001.
50. Sharp, I. D.; Xu, Q.; Liao, C. Y.; Yi, D. O.; Beeman, J. W.; Liliental-Weber, Z.; Yu, K. M.; Zakharov, D. N.; Ager, J. W., III; Chrzan, D. C.; Haller, E. E. Stable, Freestanding Ge Nanocrystals. *J. Appl. Phys.* **2005**, *97*, 124316.
51. Buriak, J. M. Organometallic Chemistry on Silicon and Germanium Surfaces. *Chem. Rev.* **2002**, *102*, 1271–1308.
52. Bottani, C. E.; Mantini, C.; Milani, P.; Manfredini, M.; Stella, A.; Tognini, P.; Cheyssac, P.; Kofman, R. Raman, Optical-Absorption, and Transmission Electron Microscopy Study of Size Effects in Germanium Quantum Dots. *Appl. Phys. Lett.* **1996**, *69*, 2409–2411.
53. Jellison Jr, G. E.; Modine, F. A. Parameterization of the Optical Functions of Amorphous Materials in the Interband Region. *Appl. Phys. Lett.* **1996**, *69*, 371–373.